European Journal of Chemistry

View Journal Online
View Article Online

# Crystal structure and supramolecular features of *O*-ethyl pivaloylcarbamothioate: insights from Hirshfeld surface and energy framework analyses

Salih Uslu [1], Ummuhan Solmaz [1,2,*] and Hakan Arslan [1]

[1] *Department of Chemistry, Faculty of Science, Mersin University, Mersin, TR 33343, Türkiye*
[2] *Department of Chemistry and Chemical Processing Technologies, Technical Science Vocational School, Mersin University, TR 33343 Mersin, Türkiye*

* *Corresponding author at: Department of Chemistry and Chemical Processing Technologies, Technical Science Vocational School, Mersin University, TR 33343 Mersin, Türkiye.*
*e-mail: ummuhansolmaz@mersin.edu.tr (U. Solmaz).*

RESEARCH ARTICLE

10.5155/eurjchem.16.4.370-378.2722

Received: 26 September 2025
Received in revised form: 21 October 2025
Accepted: 9 November 2025
Published online: 31 December 2025
Printed: 31 December 2025

KEYWORDS

Interaction energies
Crystal structure analysis
Hirshfeld surface analysis
Intermolecular interactions
Supramolecular structures
*O*-ethyl pivaloylcarbamothioate

ABSTRACT

The crystal structure of *O*-ethyl pivaloylcarbamothioate has been determined by single-crystal X-ray diffraction. The compound crystallizes in the orthorhombic crystal system, the space group *Pbca*, with unit-cell dimensions $a$ = 10.144(9) Å, $b$ = 10.230(6) Å, $c$ = 19.934(19) Å. The unit-cell volume is 2069(3) Å$^3$ with $Z$ = 8 at 298.15(2) K. A crystal specimen of size 0.241 × 0.217 × 0.124 mm$^3$ was used for data collection using CuKα radiation (λ = 1.54178 Å). The measured reflections (25,062 in total) covered the index ranges $-12 \le h \le 12$, $-12 \le k \le 13$, and $-25 \le l \le 25$, of which 2246 were unique (*R*int = 0.1349, *R*sigma = 0.0658). The refinement converged with the final values $R_1$ = 0.0942 [I > 2σ(I)] and wR2 = 0.2485 (all data), giving a calculated density of 1.216 g/cm$^3$ and the absorption coefficient μ = 2.506 mm$^{-1}$. The crystal structure of the title compound is stabilized by a hierarchical supramolecular architecture involving both classical (N-H···O) and non-classical (C-H···O, C-H···N, C-H···S) hydrogen bonds, giving rise to triangular, *zigzag*, and cyclic motifs as well as $R_2^2(9)$ and $R_4^2(24)$ synthons. Hirshfeld surface and fingerprint analyses confirm that H···H contacts dominate the packing, whereas directional H···O and H···S interactions play a crucial role in lattice cohesion. Interaction energy calculations further reveal that electrostatic and dispersion forces are the main contributors to the stabilization of the three-dimensional framework.

**Cite this**: *Eur. J. Chem.* **2025**, *16(4)*, 370-378 **Journal website**: www.eurjchem.com

## 1. Introduction

In organic chemistry, thiocarbamates (also known as thiourethanes) form a class of organosulfur compounds in which the sulfur atom substitutes for the oxygen atom of carbamates, as reflected by the 'thio-' prefix. These compounds exist in two isomeric forms: O-thiocarbamates and S-thiocarbamates. Thiocarbamates exhibit a wide spectrum of pharmacological and agrochemical activities [1]. Pharmacologically, they show antibacterial [2-5], antifungal [2-4,6], antiviral [2-4,7], and anesthetic [2-4,8] properties, with several marketed drugs, such as Tolnaftate (O-2-naphthyl *N*,*N*-dimethylthiocarbamate) (antifungal agent), Tolciclate (O-(o-chlorocinnamyl) *N*,*N*-dimethylthiocarbamate) (antifungal agent), and Goitrin (5-vinyl-2-oxazolidinethione) (thyroid hormone inhibitor) [9]. Beyond their pharmaceutical relevance, thiocarbamates are widely employed in agriculture as pesticides, with representative examples of pesticides including Thiobencarb (S-(4-chlorobenzyl)diethylcarbamothioate) (insecticide), Orbencarb (S-butyl *N*-butylcarbamothioate) (herbicide), and Molinate (S-ethyl hexahydro-1*H*-azepine-1-carbothioate) (herbicide) [2-4,8,10-12]. This versatility underscores their significance in both medicinal and agrochemical contexts. Owing to this remarkable biological potential, thiocarbamates have attracted considerable attention from academic and industrial researchers [13-19]. A notable but less explored subclass is the *N*-acyl-thiocarbamic-O-alkyl esters, which, despite their straightforward synthetic accessibility, have been largely overlooked as chelating ligands in coordination chemistry [20]. These types of compounds were first reported in 1874 and later identified in 1895 [21,22].

Structurally, the carbamothioate motif plays a central role, offering a versatile framework for the design of biologically active molecules [1]. *N*-alkoxy- or aroxy-sulfonylcarbamates and thiocarbamates can be obtained via the addition of alcohols or thiols to alkoxy- or aroxysulfonyl isocyanates [2]. *N*-acyl-thiocarbamic-O-alkyl esters gained particular attention in the 1960s in the context of heterocyclic chemistry [23-26]. More recently, they have been proposed as intermediates for the regioselective and chemoselective deoxygenation of primary and secondary aliphatic alcohols [27]. Numerous synthetic approaches have been described, among which isocyanide-based methodologies are among the most widely documented [13,28-30].


ISSN 2153-2249 (Print) / ISSN 2153-2257 (Online) 
https://dx.doi.org/10.5155/eurjchem.16.4.370-378.2722

**Table 1.** Crystal data and structure refinement for the title compound.

| Parameters | Value |
|---|---|
| Empirical formula | $C_8H_{15}NO_2S$ |
| Formula weight | 189.27 |
| Temperature (K) | 298.15(2) |
| Crystal system | Orthorhombic |
| Space group | *Pbca* |
| a (Å) | 10.144(9) |
| b (Å) | 10.230(6) |
| c (Å) | 19.934(19) |
| Volume (Å$^3$) | 2069(3) |
| Z | 8 |
| $\rho_{calc}$ (g/cm$^3$) | 1.216 |
| μ (mm$^{-1}$) | 2.506 |
| F(000) | 816.0 |
| Crystal size (mm$^3$) | 0.241 × 0.217 × 0.124 |
| Radiation | CuKα (λ = 1.54178 Å) |
| 2Θ range for data collection (°) | 8.872 to 159.672 |
| Index ranges | $-12 \le h \le 12$, $-12 \le k \le 13$, $-25 \le l \le 25$ |
| Reflections collected | 25062 |
| Independent reflections | 2246 [$R_{int}$ = 0.1349, $R_{sigma}$ = 0.0658] |
| Data/restraints/parameters | 2246/0/118 |
| Goodness-of-fit on F$^2$ | 1.025 |
| Final R indexes [I≥2σ (I)] | $R_1$ = 0.0942, $wR_2$ = 0.2259 |
| Final R indexes [all data] | $R_1$ = 0.1261, $wR_2$ = 0.2485 |
| Largest diff. peak/hole (e Å$^{-3}$) | 0.28/-0.38 |

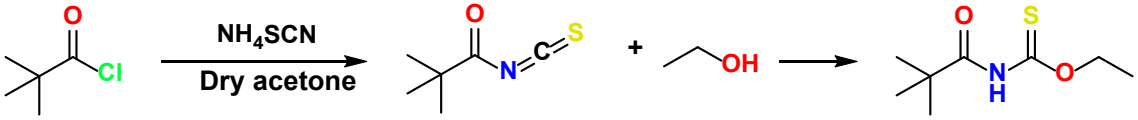


**Scheme 1.** Synthesis pathway of the title compound, *O*-ethyl pivaloylcarbamothioate.

The primary aim of this work is to elucidate the single-crystal structure of *O*-ethyl pivaloylcarbamothioate and to comprehensively analyze its supramolecular architecture. In particular, this study focuses on identifying the nature and significance of the intermolecular interactions that govern the crystal packing, using Hirshfeld surface analysis and two-dimensional fingerprint plots. Furthermore, energy framework calculations were employed to provide a quantitative understanding of the interaction energies, thereby offering deeper insights into the stabilization forces and supramolecular organization present in the crystal lattice.

## 2. Experimental

### *2.1. Synthesis of O-ethyl pivaloylcarbamothioate*

Pivaloyl chloride (0.02 mol) was dissolved in dry acetone, followed by the slow addition of ammonium thiocyanate (0.02 mol) in acetone under continuous stirring. The reaction mixture was stirred until the formation of ammonium chloride precipitate, which indicated the generation of pivaloyl isothiocyanate. Subsequently, ethanol dissolved in acetone (0.02 mol) was added dropwise to the in situ generated pivaloyl isothiocyanate, and the mixture was stirred for 12 h. The progress of the reaction was monitored by TLC using benzene: methanol (9:1, v:v) as the eluent. Upon completion, the reaction mixture was poured into 100 mL of cold water, resulting in the precipitation of *O*-ethyl pivaloylcarbamothioate [31]. The crude solid was collected by filtration. Purified colorless crystals were obtained by recrystallization from an acetone-water solvent mixture (Scheme 1).

### *2.2. Crystal structure analysis*

Single-crystal X-ray diffraction data for the title compound were obtained using a Bruker APEX–II CCD diffractometer with CuKα radiation. The structure of the title compound was determined using Olex2 software [32] in combination with Superflip structure solution software [33-35], followed by refinement using ShelXL software [36] using full-matrix least-squares techniques on $F^2$. Anisotropic displacement parameters were implemented to refine all non-H atoms, while hydrogen atoms were refined using isotropic displacement parameters and constrained by difference maps. Furthermore, the calculation of specific molecular structure parameters involved the utilization of Platon software [37] and Mercury software [38]. The crystal data and structure refinement details are summarized in Table 1.

### *2.3. Hirshfeld surface and 2D-fingerprint analyses*

The CrystalExplorer 17.5 package [39] was used to generate the Hirshfeld surface [40] and its corresponding two-dimensional fingerprint plots [41]. By employing a three-dimensional energy framework, this methodology allowed for evaluation, visualization, and analysis of intermolecular interaction energies, with a cluster radius of 3.8 Å being utilized to encompass the molecule of interest.

## 3. Results and discussions

### *3.1. Synthesis*

The synthesis of *O*-ethyl pivaloylcarbamothioate was achieved through a two-step reaction sequence involving the *in situ* generation of pivaloyl isothiocyanate, followed by nucleophilic addition of ethanol (Scheme 1). The initial reaction between pivaloyl chloride and ammonium thiocyanate in dry acetone proceeded smoothly, as indicated by the immediate formation of ammonium chloride precipitate. This observation is consistent with previous reports, confirming the efficient conversion of acyl chloride into the corresponding acyl isothiocyanate intermediate [31,42-47]. Subsequent dropwise addition of ethanol to the reaction mixture allowed for the nucleophilic attack on the electrophilic carbon of the isothiocyanate group, resulting in the formation of the desired *O*-ethyl pivaloylcarbamothioate.

**Table 2.** The bond lengths for the title compound.

| Atom | Atom | Length (Å) | Atom | Atom | Length (Å) |
|---|---|---|---|---|---|
| C1 | C3 | 1.520(6) | C3 | C4 | 1.537(7) |
| C1 | N1 | 1.394(5) | C3 | C5 | 1.530(7) |
| C1 | O1 | 1.208(5) | C3 | C6 | 1.518(6) |
| C2 | N1 | 1.386(6) | C7 | C8 | 1.487(8) |
| C2 | O2 | 1.314(6) | C7 | O2 | 1.464(6) |
| C2 | S1 | 1.628(5) | | | |

**Table 3.** The bond angles for the title compound.

| Atom | Atom | Atom | Angle (°) | Atom | Atom | Atom | Angle (°) |
|---|---|---|---|---|---|---|---|
| N1 | C1 | C3 | 115.1(4) | C5 | C3 | C4 | 109.6(5) |
| O1 | C1 | C3 | 123.3(4) | C6 | C3 | C1 | 109.5(4) |
| O1 | C1 | N1 | 121.6(4) | C6 | C3 | C4 | 109.1(4) |
| N1 | C2 | S1 | 120.3(4) | C6 | C3 | C5 | 109.5(4) |
| O2 | C2 | N1 | 112.1(4) | O2 | C7 | C8 | 107.1(5) |
| O2 | C2 | S1 | 127.6(4) | C2 | N1 | C1 | 130.1(4) |
| C1 | C3 | C4 | 110.2(4) | C2 | O2 | C7 | 117.5(4) |
| C1 | C3 | C5 | 108.9(4) | | | | |

**Table 4.** The torsion angles for the title compound.

| Atom | Atom | Atom | Atom | Angle (°) | Atom | Atom | Atom | Atom | Angle (°) |
|---|---|---|---|---|---|---|---|---|---|
| C3 | C1 | N1 | C2 | -178.8(5) | O1 | C1 | C3 | C5 | -114.9(5) |
| C8 | C7 | O2 | C2 | -176.1(5) | O1 | C1 | C3 | C6 | 4.8(7) |
| N1 | C1 | C3 | C4 | -55.9(6) | O1 | C1 | N1 | C2 | 0.5(8) |
| N1 | C1 | C3 | C5 | 64.4(5) | O2 | C2 | N1 | C1 | 17.1(7) |
| N1 | C1 | C3 | C6 | -175.9(4) | S1 | C2 | N1 | C1 | -164.9(4) |
| N1 | C2 | O2 | C7 | 177.9(4) | S1 | C2 | O2 | C7 | 0.1(7) |
| O1 | C1 | C3 | C4 | 124.8(5) | | | | | |

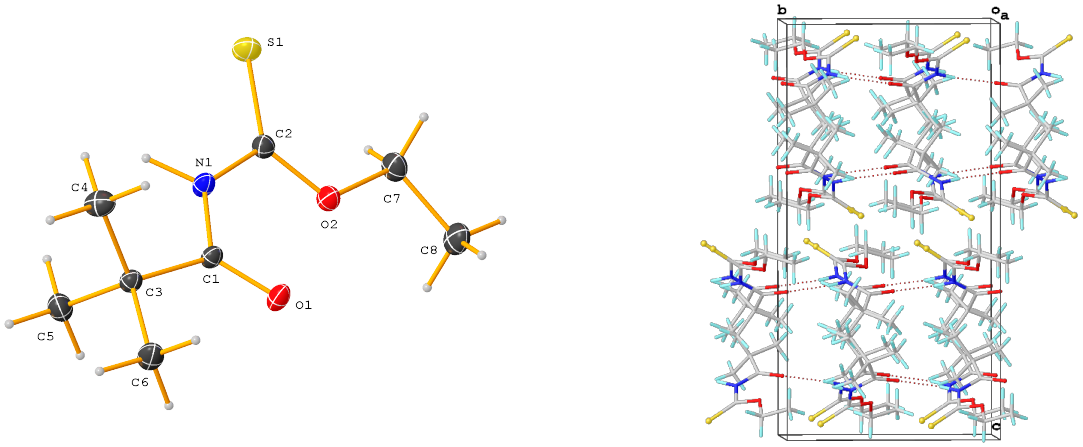


(a) (b)

**Figure 1.** (a) Molecular structure and (b) unit cell diagram of the title compound.

The reaction required extended stirring (12 h) to ensure complete consumption of the intermediate, which was monitored by TLC using a benzene:methanol (9:1, v:v) solvent system. The precipitation of the product upon pouring the reaction mixture into cold water confirmed the formation of the carbamothioate derivative. The crude product was purified by recrystallization from an acetone-water solvent mixture, yielding an analytically pure *O*-ethyl pivaloylcarbamothioate suitable for single-crystal growth and subsequent structural characterization.

### *3.2. Molecular structure and supramolecular assemblies*

The experimentally determined bond lengths, bond angles, and torsion angels for *O*-ethyl pivaloylcarbamothioate are listed in Tables 2-4. The intermolecular hydrogen bonding interactions for the title compound are summarized in Table 5. The molecular structure and unit cell diagram of the title compound are shown in Figure 1. The geometric parameters point to a molecule in which two distinct carbonyl/thiocarbonyl-type centres (C1=O1 and C2=S1 environments) are conjugated with an amide nitrogen, giving rise to partial delocalization and marked planarity at the corresponding carbon centres.

The C1–O1 bond length is 1.208(5) Å (Table 2), a value consistent with a typical C=O double bond in an acyl group and indicative of significant double-bond character [48,49]. The bond angles around C1 (N1–C1–C3 = 115.1(4)°, O1–C1–C3 = 123.3(4)° and O1–C1–N1 = 121.6(4)°) sum to ≈360° and indicate a trigonal planar geometry at C1, as expected for an $sp^2$-hybridized carbonyl carbon. The relatively large O1–C1–N1 angle (121.6°) and the N1–C1 bond length of 1.394(5) Å (Table 2) together suggest partial C1–N1 double-bond character due to resonance donation of the N lone pair into the adjacent carbonyl, consistent with amide-like conjugation.

The C2–S1 distance is 1.628(5) Å (Table 2). This short C–S separation is characteristic of a thiocarbonyl bond with considerable double-bond character (typical C=S distances fall near ~1.60–1.66 Å [48-51]), rather than a normal single C–S (≈1.75–1.82 Å [48]). The angles at C2 (N1–C2–S1 = 120.3(4)°, O2–C2–N1 = 112.1(4)° and O2–C2–S1 = 127.6(4)°) again indicate an essentially planar (trigonal) geometry, consistent with $sp^2$ hybridization and conjugation of the C2 centre with adjacent heteroatoms.

**Table 5.** Intermolecular hydrogen bonding interactions for the title compound *.

| D-H···A | d(D-H), Å | d(H···A), Å | d(D···A), Å | ∠ D-H···A, ° |
|---|---|---|---|---|
| N1–H1···O1 $^{i}$ | 0.98(6) | 2.13(6) | 3.103(6) | 169(6) |
| C4–H4C···O1 $^{i}$ | 0.96 | 2.55 | 3.448(7) | 155 |

* Symmetry code: $^{i}$ 3/2-*x*, 1/2+*y*, *z*.

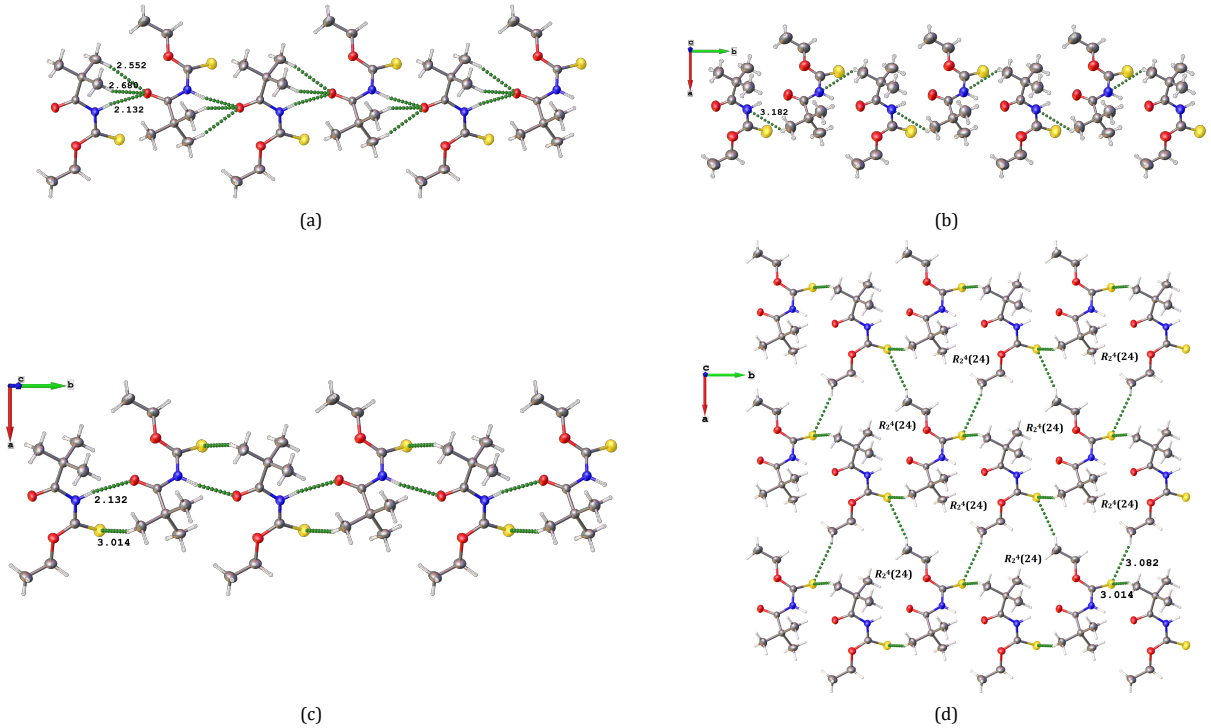


(a) (b) (c) (d)

**Figure 2.** Intermolecular hydrogen bonding interactions in the crystal structure of the title compound: (a) C4-H4C···O1, C5-H5A···O1, and N1-H1···O1 hydrogen bonds; (b) C6-H6C···N1 interactions; (c) $R_2^2(9)$ synthon; and (d) $R_4^2(24)$ synthon.

The comparatively large O2–C2–S1 angle (127.6°) further reflects the electronic distribution around the thiocarbonyl carbon, where the sulfur and oxygen substituents influence bond angles via their differing sizes and electron-donating/withdrawing effects.

The two N–C bond lengths (C1–N1 = 1.394(5) Å and C2–N1 = 1.386(6) Å, Table 2), are very similar and shorter than a typical single C–N bond (~1.47 Å [48-51]) but longer than a formal C=N double bond, consistent with partial double-bond character resulting from conjugation of the nitrogen lone pair with both the carbonyl (C1=O1) and the thiocarbonyl (C2=S1) moieties. The wide C2–N1–C1 angle of 130.1(4)° (Table 3) supports this picture: enlargement of this angle is typical when the nitrogen is involved in conjugation with adjacent $sp^2$ centres and adopts a planar disposition to maximize overlap with the neighbouring π systems.

Bond lengths within the alkyl portion attached to C3 (C3–C4 = 1.537(7) Å, C3–C5 = 1.530(7) Å, C3–C6 = 1.518(6) Å, Table 2) fall within normal C–C single-bond ranges (~1.50–1.54 Å [48]) and indicate saturated ($sp^3$) character for this part of the molecule. The C7–O2 length of 1.464(6) Å (Table 2) is typical for a C–O single bond to an alkyl/ether-type oxygen and slightly longer than purely $sp^2$ C–O bonds, consistent with the O2 atom linking an alkyl group (C7) to the carbamothioate framework.

The angles around C3 (C1–C3–C4 = 110.2(4)°, C1–C3–C5 = 108.9(4)°, C5–C3–C4 = 109.6(5)° *etc.*, Table 3) are close to the tetrahedral ideal (≈109.5°), consistent with $sp^3$ hybridization at C3. Around the O2–C7–C8 fragment, O2–C7–C8 = 107.1(5)° is slightly compressed relative to the tetrahedral values, which can be rationalized by the electronegativity of O2 and the steric demands of the adjacent substituents. Similarly, the O2–C2–N1 angle of 112.1(4)° versus the larger O2–C2–S1 angle (127.6°) reflects the differing steric and electronic requirements of oxygen and sulfur substituents at the thiocarbonyl carbon.

Taken together, the bond distances and angles indicate two conjugated acyl/thiocarbonyl centres connected through a planar nitrogen atom, giving partial π-delocalization across the N–C(=O)/C(=S) framework. The presence of a relatively short C2–S2 separation (thiocarbonyl character) and shortened N–C bonds support strong resonance stabilization of the carbamothioate moiety.

The crystal structure of the title compound reveals a rich supramolecular architecture formed through multiple hydrogen bonding interactions with distinct geometrical motifs (Figure 2). The C4-H4···O1 (2.552 Å), C5-H5A···O1 (2.680 Å), and N1-H1···O1 (2.132 Å) contacts generate a triangular pyramidal motif. Within this arrangement, the conventional N1-H1···O1 hydrogen bond is the shortest and strongest interaction, while the C-H···O contacts act as auxiliary linkers that complete the three-dimensional triangular pyramidal assembly (Figure 2a). A weaker C6-H6C···N1 interaction (3.182 Å) gives rise to a *zigzag* motif. Although such C-H···N interactions are generally weaker than classical N-H···O bonds, they provide an important contribution to overall packing by propagating chain-like supramolecular patterns along the lattice (Figure 2b). The $R_2^2(9)$ synthon is generated through the combination of the strong N1-H1···O1 hydrogen bond (2.132 Å) and the weaker C6-H6C···S1 interaction (3.014 Å). The short and directional N-H···O contact serves as the main stabilizing force, while the longer C-H···S bond complements this interaction, allowing the formation of a cyclic hydrogen-bonded dimer (Figure 2c).

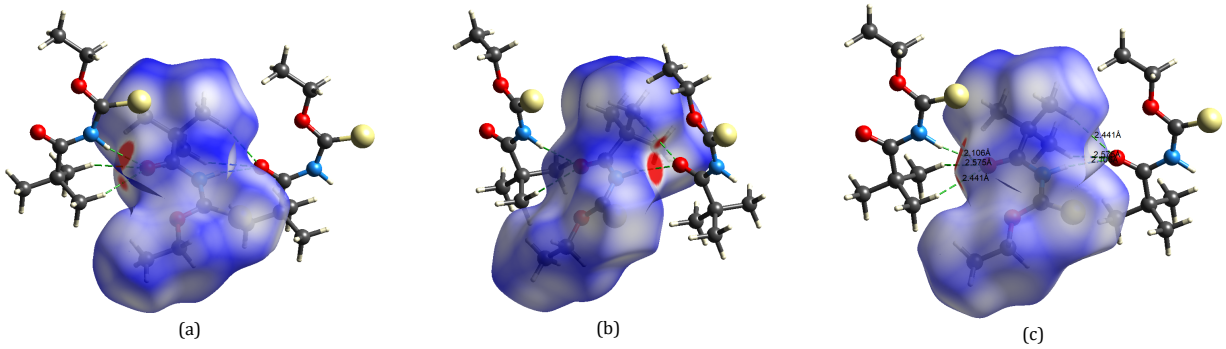


(a) (b) (c)

**Figure 3.** Intermolecular interactions in the structure of the title compound as visualized by $d_{norm}$ surface plots: (a) left-side view, (b) right-side view, and (c) detailed representation of hydrogen-bonding interactions with bond distances.

A larger supramolecular motif, the $R_4^2(24)$ synthon, is established through C8-H8A···S2 (3.082 Å) and C6-H6C···S2 (3.014 Å) interactions, involving four hydrogen bonds. This extended motif connects multiple molecules into a higher-order assembly, reinforcing the three-dimensional supra-molecular framework (Figure 2d).

In general, the combination of classical (N-H···O) and non-classical (C-H···O, C-H···N, and C-H···S) interactions generates a hierarchical supramolecular architecture in the title compound. The presence of both triangular and *zigzag* motifs, along with $R_2^2(9)$ and $R_4^2(24)$ synthons, highlights the cooperative role of strong and weak hydrogen bonds in directing the crystal packing and stabilizing the lattice.

### *3.3. Hirshfeld surface and two-dimensional fingerprint analyses*

The intermolecular interactions of the title compound were further elucidated through Hirshfeld surface (HS) and two-dimensional fingerprint (2D-FP) analyses, performed with CrystalExplorer 17.5 [39,40,]. The $d_{norm}$ surfaces mapped over the range of -0.1000 to 1.0000 a.u. provide a clear visualization of the regions where close contacts occur (Figure 3). These spots correspond to significant hydrogen-bonding interactions, which agree with the crystallographic findings.

The red spots on the $d_{norm}$ surface correspond to short and significant hydrogen-bonding interactions, particularly the N-H···O and C-H···O contacts, which are consistent with the crystallographic data. The left- (Figure 3a) and right-side (Figure 3b) views highlight the distribution of these interactions around the molecular surface, while the detailed plot confirms the involvement of strong and weak hydrogen bonds with their corresponding bond distances. In particular, the $d_{norm}$ surface visualization (Figure 3c) emphasizes the dominant N-H···O hydrogen bond (H···O distance = 2.106 Å), along with additional C-H···O interactions (2.575 and 2.441 Å). These short contacts are consistent with the X-ray diffraction results, where the supramolecular assembly was shown to be stabilized by a combination of strong N-H···O and weaker C-H···O interactions. The correspondence between the HS red spots and the experimentally observed bond distances demonstrates the reliability of the Hirshfeld approach in confirming the packing forces that govern the crystal architecture. Both methods highlight that the N–H···O interaction is the most significant contributor to lattice cohesion, while C–H···O and C–H···S contacts act as secondary linkers, shaping the overall three-dimensional framework.

To further explore the nature of these intermolecular contacts, a series of HS properties were examined (Figure 4). The $d_i$ (0.8884-2.5162 Å) and $d_e$ (0.8874-2.5354 Å) surfaces describe the internal and external distances from the Hirshfeld surface to the nearest nuclei, respectively, and help to distinguish the donor–acceptor interactions. The shape index (-1.000-1.0000 Å) and curvedness (-4.0000-0.4000 Å) maps provide additional insight into the overall molecular packing, indicating π···π stacking features are absent, whereas C-H···O/N/S hydrogen bonds dominate the packing arrangement. The fragment patch surface (0.0000-15.0000 Å) reveals the local environments and highlights the contribution of different interaction fragments around the central molecule.

Figure 4 presents the two-dimensional (2D) fingerprint plots for the title compound, highlighting intermolecular interactions that contribute more than 2% to the total Hirshfeld surface. In these graphs, the hydrogen bond acceptor regions are represented by points with $d_e > d_i$, while the donor regions are identified by $d_i > d_e$ [41,52,53]. The analysis indicates that H···H contacts are the most dominant, accounting for 58.90% of the Hirshfeld surface. These interactions appear as sharp spikes centered around $d_e \approx d_i \approx 1.1$ Å, reflecting the van der Waals contacts between hydrogen atoms, which play a major role in packing efficiency but do not involve directional bonding. The H···S/S···H contacts contribute 17.40% of the surface and display a characteristic wing-like pattern ($d_e \approx d_i \approx 1.8$ Å), indicative of weaker C–H···S hydrogen bonding interactions that act as secondary stabilizing forces within the crystal lattice. Similarly, H···O/O···H contacts account for 16.40% of the Hirshfeld surface and are represented by two sharp spikes ($d_e \approx d_i \approx 1.2$ Å), corresponding to the strong directional N–H···O and C–H···O hydrogen bonds observed in the XRD structure. Minor contributions arise from C···H/H···C (4.00%) and N···H/H···N (2.10%) interactions, reflecting less frequent but structurally relevant contacts that complement the primary hydrogen bonding network.

Overall, the 2D fingerprint plots quantitatively confirm that the crystal packing is dominated by H···H van der Waals interactions (58.90%), while directional hydrogen bonds-especially H···O (16.40%) and H···S (17.40%) play a key role in forming the supramolecular architecture. These results are consistent with the Hirshfeld surface and X-ray diffraction analyses, illustrating the cooperative contributions of strong and weak interactions in stabilizing the three-dimensional crystal structure.

### *3.4. Interaction energies*

The intermolecular interactions in the crystal structure of the title compound were further investigated using CrystalExplorer 17.5, which calculates interaction energies based on electron density wavefunctions [39,54,55]. This approach allows the decomposition of the total interaction energy ($E_{tot}$) into its components: electrostatic ($E_{ele}$), polarization ($E_{pol}$), dispersion ($E_{dis}$), and repulsion ($E_{rep}$) [45,56,57]. Scale factors of 1.057, 0.740, 0.871, and 0.618 were applied for $k_{ele}$, $k_{pol}$, $k_{dis}$, and $k_{rep}$, respectively.

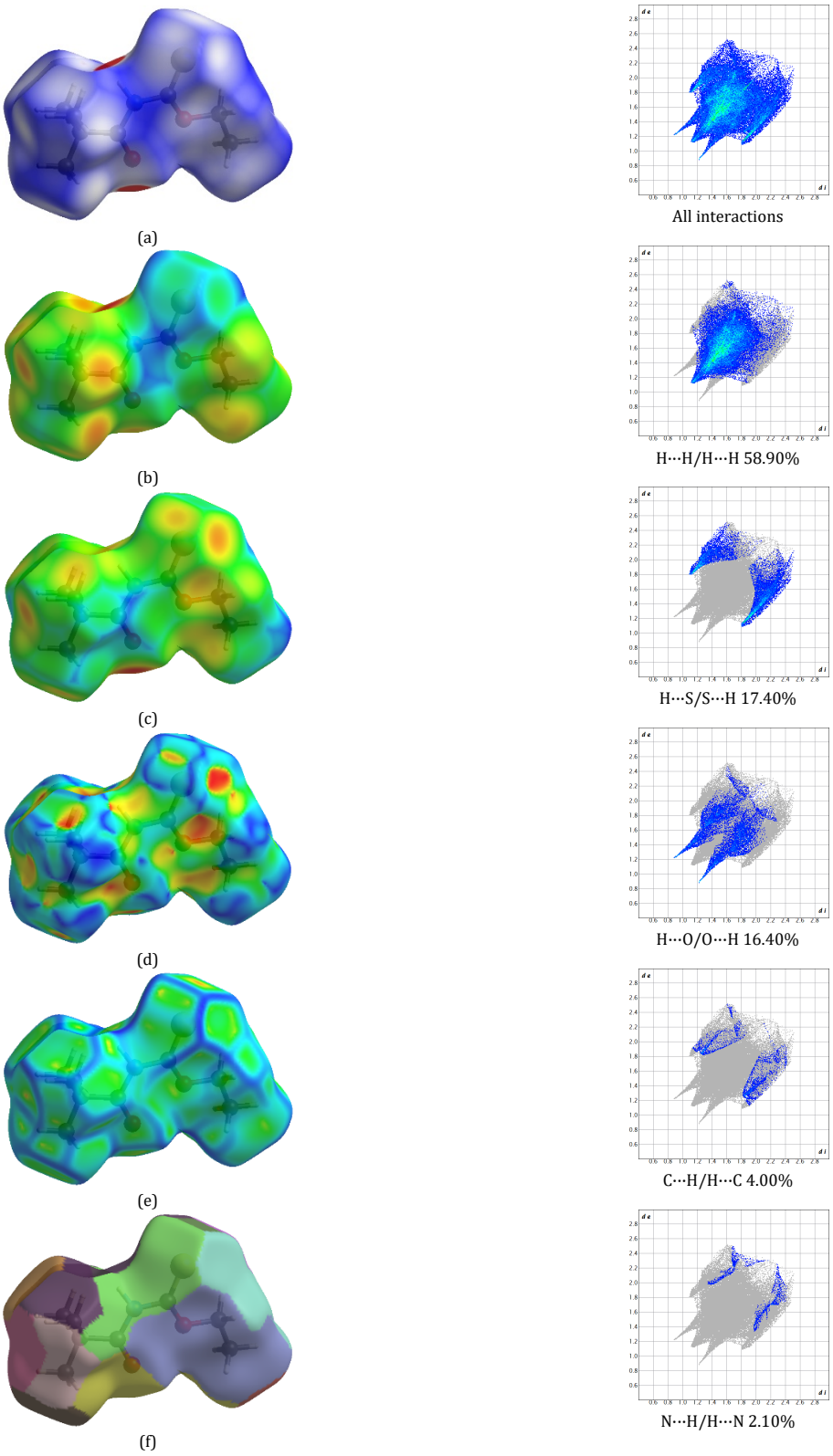


**Figure 4.** Visual representations of Hirshfeld surfaces: (a) $d_{norm}$, (b) $d_i$, (c) $d_e$, (d) shape index, (e) curvedness, and (f) fragment patch; 2D-fingerprint plots for the title compound.

The calculations of the interaction energy based on the molecular pairs of the title compound are illustrated in Figure 5. Table 6 summarizes the calculated interaction energies for selected molecular pairs. The molecule highlighted in green exhibits the strongest total interaction energy of -41.5 kJ/mol at a centroid distance of 5.42 Å, primarily due to significant electrostatic (-33.5 kJ/mol) and dispersion (-32.0 kJ/mol) contributions, despite the repulsive term (46.4 kJ/mol). In contrast, the molecule highlighted in purple, at a larger centroid distance of 7.92 Å, demonstrates the weakest total interaction energy of -2.6 kJ/mol, reflecting minimal noncovalent interactions at longer intermolecular separations.

**Table 6.** The interaction energies of title compound have been calculated in kj/mol.

| Color [i] | N [ii] | Symop | R [iii] | $E_{ele}$ | $E_{pol}$ | $E_{dis}$ | $E_{rep}$ | $E_{tot}$ |
|---|---|---|---|---|---|---|---|---|
| | 2 | *x*, *y*, *z* | 10.14 | 0.5 | -0.1 | -4.2 | 0.4 | -2.9 |
| | 2 | -*x*+1/2, *y*+1/2, *z* | 9.79 | -4.3 | -0.7 | -5.9 | 7.3 | -5.7 |
| | 1 | -*x*, -*y*, -*z* | 6.67 | -5.7 | -1.4 | -24.1 | 11.9 | -20.7 |
| | 2 | -*x*+1/2, y+1/2, *z* | 5.42 | -33.5 | -9.3 | -32.0 | 46.4 | -41.5 |
| | 2 | *x*+1/2, -*y*+1/2, -*z* | 7.31 | -8.4 | -2.0 | -13.0 | 13.4 | -13.3 |
| | 2 | *x*+1/2, *y*, -*z*+1/2 | 7.18 | -0.7 | -1.0 | -22.1 | 10.4 | -14.3 |
| | 2 | -*x*, *y*+1/2, -*z*+1/2 | 9.96 | -1.1 | -0.3 | -8.1 | 3.7 | -6.1 |
| | 2 | -*x*, *y*+1/2, -*z*+1/2 | 7.92 | -0.3 | -0.1 | -2.7 | 0.1 | -2.6 |
| | 1 | -*x*, -*y*, -*z* | 9.21 | 3.5 | -0.5 | -3.4 | 4.1 | 2.9 |
| Total | | | | -50.0 | -15.4 | -115.5 | 97.7 | -104.2 |

[i] The correlation between the molecule and color (Figure 5).
[ii] Number of pairs interacting with the central molecule (N).
[iii] The distance between centroids of molecules (R).

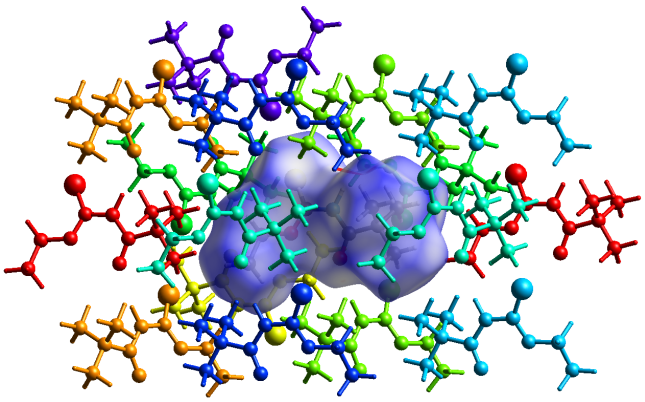

**Figure 5.** Interaction energy calculations based on molecular pairs for the title compound.

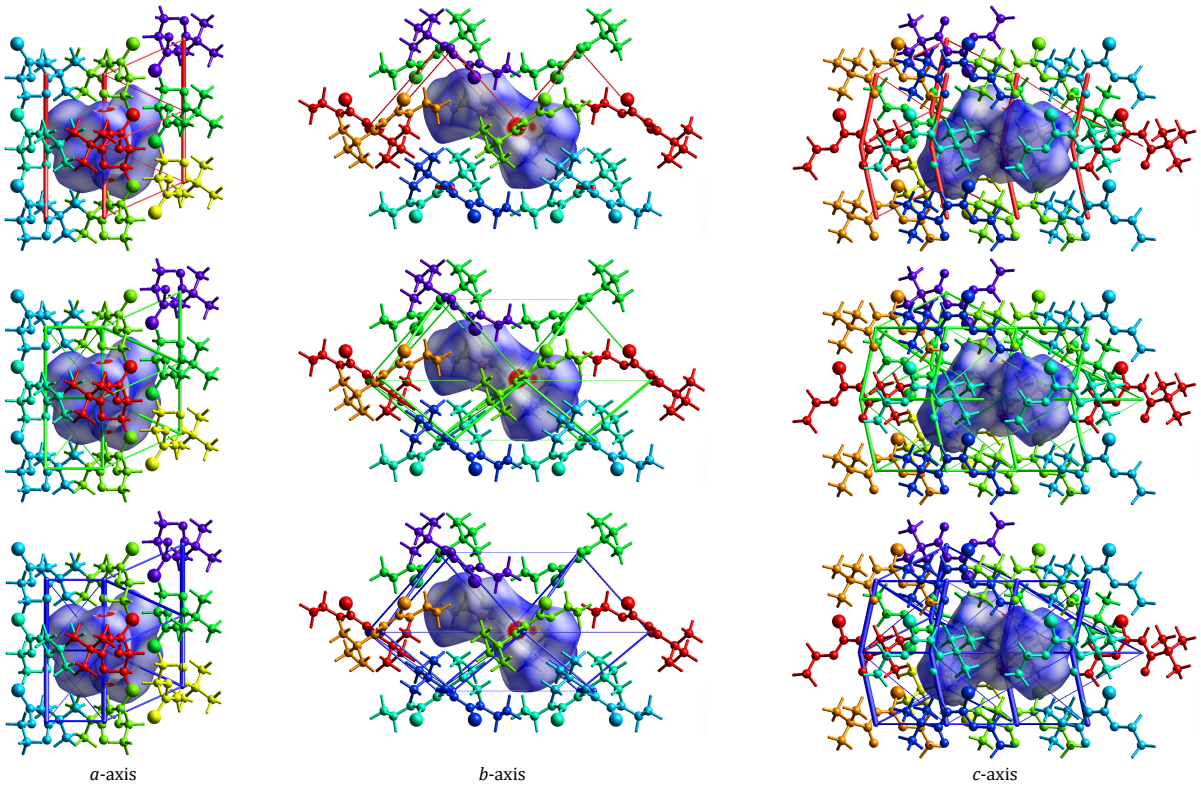


**Figure 6.** Coulomb energy (top), dispersion energy (middle), and total interaction energy (bottom) mapped along the crystallographic *a*-, *b*-, and *c*-axes for the molecules within the unit cell of the title compound.

The electrostatic, polarization, dispersion, and repulsion energies were found to be -50.0, -15.4, -115.5 and 97.7 kJ/mol, respectively, resulting in a total interaction energy of -104.2 kJ/mol (Table 6). These values indicate that the strong lattice stabilization arises predominantly from electrostatic and dispersion interactions, which act cooperatively to counter-balance the repulsive contributions.

The Coulomb, dispersion, and total interaction energies of the molecules within the unit cell of the title compound were mapped along the crystallographic *a*-, *b*-, and *c*-axes to visualize the directional contributions of different intermolecular interactions (Figure 6).

## 4. Conclusions

The measured geometric parameters are fully consistent with a carbamothioate structure in which the nitrogen atom participates in conjugation with both a carbonyl and a thiocarbonyl centre, producing partial double-bond character in N–C bonds and planar geometries at C1 and C2. These stereoelectronic properties rationalize the observed molecular shape and provide a structural basis for supramolecular contacts and packing motifs that will be further investigated by Hirshfeld surface analysis and energy framework calculations.

The crystal structure of the title compound exhibits a hierarchical supramolecular framework governed by both classical (N–H···O) and non-classical (C–H···O, C–H···N, and C–H···S) hydrogen bonds. Triangular and *zigzag* motifs, together with the $R_2^2(9)$ and $R_4^2(24)$ synthons, demonstrate how strong directional and weaker auxiliary interactions act cooperatively to stabilize the three-dimensional packing. These findings highlight the interplay of multiple hydrogen-bonding patterns in directing the overall lattice architecture.

The Hirshfeld surface and 2D fingerprint analyzes confirmed that the crystal packing of the title compound is primarily governed by H···H contacts, which contribute nearly 59% of the total surface. Directional hydrogen bonds, especially N–H···O and C–H···O interactions, play a dominant role in lattice cohesion, while C–H···S contacts act as secondary stabilizing forces. The results are fully consistent with the X-ray diffraction data, highlighting the cooperative contributions of strong and weak intermolecular interactions in stabilizing the three-dimensional supramolecular architecture.

The interaction energy analysis revealed that the crystal packing of the title compound is mainly stabilized by cooperative electrostatic and dispersion forces, which counter-balance repulsive contributions. The strongest molecular pair exhibited a stabilization energy of –41.5 kJ/mol, while weaker interactions were observed at longer distances. In general, electrostatic and dispersion interactions play the dominant role in the lattice stability of the title compound.

## Acknowledgements

This study is supported by Mersin University Scientific Research Projects Coordination Unit (Project Number: 2024-TP3-5145) and the work constitutes a part of Salih Uslu's PhD thesis. In addition, this work was also partially supported by the Advanced Technology Education, Research and Application Center of Mersin University, Mersin, Türkiye.

## Supporting information

CCDC-2493071 contains the supplementary crystallographic data for this paper. These data can be obtained free of charge via www.ccdc.cam.ac.uk/data_request/cif, or by e-mailing data_request@ccdc.cam.ac.uk, or by contacting The Cambridge Crystallographic Data Centre, 12 Union Road, Cambridge CB2 1EZ, UK; fax: +44(0)1223-336033.

## Disclosure statement

Conflict of interests: The authors declare that they have no conflict of interest.
Ethical approval: All ethical guidelines have been adhered.
Sample availability: Sample of the compound are available from the author.

## CRediT authorship contribution statement

Conceptualization: Salih Uslu, Ummuhan Solmaz, Hakan Arslan; Methodology: Ummuhan Solmaz, Hakan Arslan; Validation: Ummuhan Solmaz, Hakan Arslan; Formal Analysis: Salih Uslu, Ummuhan Solmaz, Hakan Arslan; Investigation: Salih Uslu, Ummuhan Solmaz, Hakan Arslan; Resources: Salih Uslu, Ummuhan Solmaz, Hakan Arslan; Data Curation: Salih Uslu, Ummuhan Solmaz, Hakan Arslan; Writing - Original Draft: Salih Uslu, Ummuhan Solmaz, Hakan Arslan; Writing - Review and Editing: Ummuhan Solmaz, Hakan Arslan; Visualization: Ummuhan Solmaz, Hakan Arslan; Funding acquisition: Hakan Arslan; Supervision: Hakan Arslan; Project Administration: Hakan Arslan.

## Funding

Mersin Üniversitesi
http://dx.doi.org/10.13039/501100004172

## ORCID and Email

Salih Uslu
salih.uslu.tr@gmail.com
https://orcid.org/0009-0007-5504-3189
Ummuhan Solmaz
ummuhansolmaz@mersin.edu.tr
https://orcid.org/0000-0002-3697-577X
Hakan Arslan
hakan.arslan@mersin.edu.tr
https://orcid.org/0000-0003-0046-9442

## References

[1]. Khalaj, M. Synthesis of carbamothioate derivatives via a copper catalyzed thiocarboxamidation of aryl iodides. *Monatsh. Chem.* **2020**, *151* (6), 945–952.
[2]. Beji, M.; Sbihi, H.; Baklouti, A.; Cambon, A. Synthesis of F-alkyl N-sulfonyl carbamates and thiocarbamates. *J. Fluor. Chem.* **1999**, *99*, 17–24.
[3]. Heyns, A. J.; Carter, G. A.; Rothwell, K.; Waın, R. L. Investigations on fungicides: The systemic fungicidal activity of certain *N*-carboxymethyl dithiocarbamic acid derivatives. *Annals. Applied Biology* **1966**, *57* (1), 33–51.
[4]. Padiya, K. J.; Gavade, S.; Kardile, B.; Tiwari, M.; Bajare, S.; Mane, M.; Gaware, V.; Varghese, S.; Harel, D.; Kurhade, S. Unprecedented "In Water" Imidazole Carbonylation: Paradigm Shift for Preparation of Urea and Carbamate. *Org. Lett.* **2012**, *14* (11), 2814–2817.
[5]. Bowden, K.; Bromley, K. Reactions of carbonyl compounds in basic solutions. Part 15. The alkaline hydrolysis of N-methyl, N-phenyl and bicyclo lactams, penicillins and N-alkyl-N-methylacetamides. *J. Chem. Soc., Perkin Trans. 2.* **1990**, 2111.
[6]. Erian, A. W.; Sherif, S. M. The chemistry of thiocyanic esters. *Tetrahedron* **1999**, *55*, 7957–8024.
[7]. Wood, T. F.; Gardner, J. H. The Synthesis of Some Dialkylaminoalkyl Arylthiourethans and Thioureas[1]. *J. Am. Chem. Soc.* **1941**, *63* (10), 2741–2742.
[8]. Goel, A.; Mazur, S. J.; Fattah, R. J.; Hartman, T. L.; Turpin, J. A.; Huang, M.; Rice, W. G.; Appella, E.; Inman, J. K. Benzamide-based thiolcarbamates: a new class of HIV-1 NCp7 inhibitors. *Bioorg. Med. Chem. Lett.* **2002**, *12*, 767–770.
[9]. Tan, D.; Ng, Z. X.; Ganguly, R.; Li, Y.; Soo, H. S.; Mohamed, S.; García, F. Investigating the solid-state assembly of pharmaceutically-relevant *N*,*N*-dimethyl-*O*-thiocarbamates in the absence of labile hydrogen bonds. *CrystEngComm.* **2020**, *22* (48), 8290–8298.
[10]. Mampuys, P.; Zhu, Y.; Sergeyev, S.; Ruijter, E.; Orru, R. V.; Van Doorslaer, S.; Maes, B. U. Iodide-Catalyzed Synthesis of Secondary Thiocarbamates from Isocyanides and Thiosulfonates. *Org. Lett.* **2016**, *18* (12), 2808–2811.
[11]. Lindgren, B.; Lindgren, G.; Artursson, E.; Puu, G.; Fredriksson, J.; Andersson, M. Acetylcholinesterase Inhibition by Sulphur and Selenium Heterosubstituted Isomers of*N*,*N*-Diethylcarbamyl Choline and Carbaryl. *J. Enzyme. Inhibition* **1985**, *1* (1), 1–11.
[12]. Ishikawa, K.; Okuda, I.; Kuwatsuka, S. Metabolism of Benthiocarb (4-Chlorobenzyl N,N-Diethylthiolcarbamate) in Mice. *Agricul. Biol. Chem.* **1973**, *37* (1), 165–173.
[13]. Wei, W.; Bao, P.; Yue, H.; Liu, S.; Wang, L.; Li, Y.; Yang, D. Visible-Light-Enabled Construction of Thiocarbamates from Isocyanides, Thiols, and Water at Room Temperature. *Org. Lett.* **2018**, *20* (17), 5291–5295.
[14]. Weijlard, J.; Tishler, M. Some New Choline Type Thiols. *J. Am. Chem. Soc.* **1951**, *73* (4), 1497–1500.
[15]. Movassagh, B.; Soleiman-Beigi, M. Synthesis of Thiocarbamates from Thiols and Isocyanates Under Catalyst- and Solvent-Free Conditions. *Monatsh. Chem.* **2008**, *139* (2), 137–140.
[16]. Mizuno, T.; Iwai, T.; Ishino, Y. Solvent-assisted thiocarboxylation of amines and alcohols with carbon monoxide and sulfur under mild conditions. *Tetrahedron* **2005**, *61* (38), 9157–9163.

[17]. Kim, H.; Lee, A. One-pot synthesis of carbamates and thiocarbamates from Boc-protected amines. *Tetrahedron. Letters.* **2016**, *57* (44), 4890–4892.
[18]. Zhang, Q.; Queneau, Y.; Soulère, L. Biological evaluation and docking studies of new carbamate, thiocarbamate, and hydrazide analogues of acyl homoserine lactones as Vibrio fischeri-quorum sensing modulators. *Biomolecules* **2020**, *10*, 455.
[19]. Manne, S. R.; Thalluri, K.; Giri, R. S.; Chandra, J.; Mandal, B. Ethyl 2-(*tert*-Butoxycarbonyloxyimino)-2-cyanoacetate (Boc-Oxyma): An Efficient Reagent for the Racemization Free Synthesis of Ureas, Carbamates and Thiocarbamates via Lossen Rearrangement. *Adv. Synth. Catal.* **2016**, *359* (1), 168–176.
[20]. Schroder, U.; Beyer, L.; Dietze, F.; Richter, R.; Schmidt, S.; Hoyer, E. Ligand Properties of N-Acyl-thiocarbamic-O-alkylesters - A new class of aza-analogous 1,3-thioxoketones. *J. Prakt. Chem.* **1995**, *337* (1), 184–188.
[21]. Lössner, L. Ueber die Einwirkung von Benzoylchlorid auf Rhodankalium in alkoholischer Lösung. *J. Prakt. Chem.* **1874**, *10* (1), 235–261.
[22]. Dixon, A. E. CIX.-Acidylthiocarbimides. *J. Chem. Soc., Trans.* **1895**, *67*, 1040–1049.
[23]. Sakamoto, M.; Tanaka, M.; Fukuda, A.; Aoyama, H.; Omote, Y. Synthesis and photolysis of 4-thioxoazetidin-2-ones. *J. Chem. Soc., Perkin. Trans 1* **1988**, 1353.
[24]. Whitfield, L. L.; Papadopoulos, E. P. Heterocycles from *N*-benzoylthioamides and dinucleophilic reagents. *J. Heterocyclic. Chem.* **1981**, *18* (6), 1197–1201.
[25]. Kulka, M. Synthesis of *N*-acyl-1,3-oxathiol-2-imines. *Can. J. Chem.* **1981**, *59* (11), 1557–1559.
[26]. Kristian, P.; Kutschy, P.; Dzurilla, M. Synthesis of 2,2,4-trisubstituted 2H-1,3-oxazetes from acyl isothiocyanates. *Collect. Czech. Chem. Commun.* **1979**, *44* (4), 1324–1333.
[27]. Oba, M.; Nishiyama, K. Deoxygenation of Aliphatic Alcohols via Reduction of New Thioxocarbamate Derivatives. *Synthesis* **1994**, *1994* (06), 624–628.
[28]. Wu, S.; Lei, X.; Fan, E.; Sun, Z. Thermolysis-Induced Two- or Multicomponent Tandem Reactions Involving Isocyanides and Sulfenic-Acid-Generating Sulfoxides: Access to Diverse Sulfur-Containing Functional Scaffolds. *Org. Lett.* **2018**, *20* (3), 522–525.
[29]. Sardarian, A. R.; Inaloo, I. D.; Modarresi-Alam, A. R. Highly efficient synthesis of alkyl and aryl primary thiocarbamates and dithiocarbamates under metal- and solvent-free conditions. *Mol. Divers.* **2018**, *22*, 863–878.
[30]. Grzyb, J. A.; Shen, M.; Yoshina-Ishii, C.; Chi, W.; Brown, R.; Batey, R. A. Carbamoylimidazolium and thiocarbamoylimidazolium salts: novel reagents for the synthesis of ureas, thioureas, carbamates, thiocarbamates and amides. *Tetrahedron* **2005**, *61* (30), 7153–7175.
[31]. Plutín, A. M.; Suárez, M.; Ochoa, E.; Machado, T.; Mocelo, R.; Concellón, J. M.; Rodríguez-Solla, H. Synthesis of new acyl, furoyl, and benzoylthiocarbamates as polydentate systems. Structural study of isopropyl N-(2-furoyl)thiocarbamate. *Tetrahedron* **2005**, *61* (24), 5812–5817.
[32]. Dolomanov, O. V.; Bourhis, L. J.; Gildea, R. J.; Howard, J. A.; Puschmann, H. *OLEX2*: a complete structure solution, refinement and analysis program. *J. Appl. Crystallogr.* **2009**, *42* (2), 339–341.
[33]. Palatinus, L.; Steurer, W.; Chapuis, G. Extending the charge-flipping method towards structure solution from incomplete data sets. *J. Appl. Crystallogr.* **2007**, *40* (3), 456–462.
[34]. Palatinus, L.; van der Lee, A. Symmetry determination following structure solution in*P*1. *J. Appl. Crystallogr.* **2008**, *41* (6), 975–984.
[35]. Palatinus, L.; Prathapa, S. J.; van Smaalen, S. *EDMA*: a computer program for topological analysis of discrete electron densities. *J. Appl. Crystallogr.* **2012**, *45* (3), 575–580.
[36]. Sheldrick, G. M. Crystal structure refinement with *SHELXL*. *Acta. Crystallogr. C. Struct. Chem.* **2015**, *71* (1), 3–8.
[37]. Spek, A. L. *PLATON* SQUEEZE: a tool for the calculation of the disordered solvent contribution to the calculated structure factors. *Acta. Crystallogr. C. Struct. Chem.* **2015**, *71* (1), 9–18.
[38]. Macrae, C. F.; Edgington, P. R.; McCabe, P.; Pidcock, E.; Shields, G. P.; Taylor, R.; Towler, M.; van de Streek, J. *Mercury*: visualization and analysis of crystal structures. *J. Appl. Crystallogr.* **2006**, *39* (3), 453–457.
[39]. Spackman, P. R.; Turner, M. J.; McKinnon, J. J.; Wolff, S. K.; Grimwood, D. J.; Jayatilaka, D.; Spackman, M. A. *CrystalExplorer*: a program for Hirshfeld surface analysis, visualization and quantitative analysis of molecular crystals. *J. Appl. Crystallogr.* **2021**, *54* (3), 1006–1011.
[40]. McKinnon, J. J.; Jayatilaka, D.; Spackman, M. A. Towards quantitative analysis of intermolecular interactions with Hirshfeld surfaces. *Chem. Commun.* **2007**, 3814.
[41]. Spackman, M. A.; Jayatilaka, D. Hirshfeld surface analysis. *CrystEngComm.* **2009**, *11* (1), 19–32.
[42]. Alizada, A.; Arslan, H. Experimental and theoretical studies of a thiourea derivative: 1-(4-chloro-benzoyl)-3-(2-trifluoromethyl-phenyl)thiourea. *J. Mol. Struc.* **2023**, *1279*, 134996.
[43]. Oztaslar, A.; Arslan, H. N–((2–Acetylphenyl)carbamothioyl) benzamide: Synthesis, crystal structure analysis, and theoretical studies. *Karbala. International Journal of Modern Science* **2023**, *9* (3), https://doi.org/10.33640/2405-609x.3304.
[44]. Yilmaz, E. A.; Solmaz, U.; Arslan, H. Experimental and theoretical analyses of the structural composition and supramolecular structures of selenoureas: Evaluating antioxidant activity. *J. Mol. Struct.* **2026**, *1350*, 144055.
[45]. Solmaz, U.; Keskin, E.; Arslan, H. Palladium(II) complexes of thiobenzamide derivative ligands: Synthesis, crystal structure, supramolecular architecture, Hirshfeld surface analysis, and in vitro antibacterial and antifungal activities. *J. Mol. Struct.* **2024**, *1308*, 138103.
[46]. Uysal, M. E.; Solmaz, U.; Arslan, H. Ru(II) and Ru(III) complexes containing *N*-acylthiourea ligands: Supramolecular structures and synthons, reduction, and reaction pathway of aromatic nitro compounds. *Appl. Organometal. Chem.* **2023**, *37* (7), https://doi.org/10.1002/aoc.7107.
[47]. Solmaz, U.; Arslan, H. Spectral, crystallographic, theoretical, and catalytic activity studies of the PdII complexes in different coordination modes of benzoylthiourea ligand. *J. Mol. Struct.* **2022**, *1269*, 133839.
[48]. Allen, F. H.; Kennard, O.; Watson, D. G.; Brammer, L.; Orpen, A. G.; Taylor, R. Tables of bond lengths determined by X-ray and neutron diffraction. Part 1. Bond lengths in organic compounds. *J. Chem. Soc., Perkin. Trans. 2* **1987**, S1.
[49]. Ozer, C. K.; Solmaz, U.; Arslan, H. Crystal structure, Hirshfeld surface analysis, and DFT studies of N-(2-chlorophenylcarbamothioyl) cyclohexanecarboxamide. *Eur. J. Chem.* **2021**, *12* (4), 439–449.
[50]. Gumus, I.; Solmaz, U.; Binzet, G.; Keskin, E.; Arslan, B.; Arslan, H. Supramolecular self-assembly of new thiourea derivatives directed by intermolecular hydrogen bonds and weak interactions: crystal structures and Hirshfeld surface analysis. *Res. Chem. Intermed.* **2018**, *45* (2), 169–198.
[51]. Gumus, I.; Solmaz, U.; Binzet, G.; Keskin, E.; Arslan, B.; Arslan, H. Hirshfeld surface analyses and crystal structures of supramolecular self-assembly thiourea derivatives directed by non-covalent interactions. *J. Mol. Struct.* **2018**, *1157*, 78–88.
[52]. Spackman, M. A.; McKinnon, J. J. Fingerprinting intermolecular interactions in molecular crystals. *CrystEngComm.* **2002**, 4, 378–392.
[53]. Spackman, M. A.; McKinnon, J. J.; Jayatilaka, D. Electrostatic potentials mapped on Hirshfeld surfaces provide direct insight into intermolecular interactions in crystals. *CrystEngComm.* **2008**, *10*, 377–388.
[54]. Somashekar, M. N.; Chetana, P. R.; Chethan, B. S.; Rajegowda, H. R.; Cooper, M. A.; Ziora, Z. M.; Lokanath, N. K.; Ganapathy, P. S. S.; Srinatha, B. S. Synthesis and characterization of Zinc(II) complex with ONO donor type new phenylpropanehydrazide based ligand: Crystal structure, Hirshfeld surface analysis, DFT, energy frameworks and molecular docking. *J. Mol. Struct.* **2022**, *1255*, 132429.
[55]. Clausen, H. F.; Chevallier, M. S.; Spackman, M. A.; Iversen, B. B. Three new co-crystals of hydroquinone: crystal structures and Hirshfeld surface analysis of intermolecular interactions. *New J. Chem.* **2010**, *34*, 193–199.
[56]. Keskin, E.; Solmaz, U.; Arslan, H. NNN type pincer Pd (II) complexes of pyridine-2,6-dicarboxamides: Catalytic activity and supramolecular formation. *J. Mol. Struct.* **2025**, *1322*, 140462.
[57]. Keskin, E.; Arslan, H. Synthesis, crystal structure, DFT calculations, and Hirshfeld surface analysis of an NNN pincer type compound. *J. Mol. Struct.* **2023**, *1283*, 135252.